Metal Doped Nanostructures Derived from Biomass for Supercapacitor Applications: Effect of Doping on Cyclability

Amrita De Adhikari

Abstract In the battle between industrialization and conserving the environment, ecologically viable biomass niches are in high demand. Storing and delivering energy with durability and steadiness has been crucial. Conventionally, carbonaceous materials have been used for years in supercapacitor fabrication. A sustainable supply of energy with minimum cost and huge benefits has made biomass-derived nanostructures suitable for supercapacitor applications. The design of customizable nanostructures (e.g., nanorods, nanoflowers, nanosheets, nanotubes, etc.) has been found to be dependent on dopants, the morphology of precursors, surface area parameters, and many more factors. An enormous number of biowaste and biomass materials have been employed to attain various nanostructures that are beneficial for electrochemical energy storage. Auxiliary, doping metals, and heteroatoms are found to be advantageous as they can lead to the generation of redox active sites, increased cyclability, and reduced resistance to charge transfer. The overall electronic framework has played a significant role in the stability and robustness of the nanostructure in supercapacitors. This chapter discusses the various superstructures derived from biomass, as well as their intrinsic electrochemical performance on metal doping. Metal doped nanostructured carbonaceous materials derived from replenishable, inexpensive, and environmentally friendly biomass have become the "cherry on top" in supercapacitor research communities.

Keywords Biomass · Biowaste · Metal doping · Supercapacitors · Nanostructures · Cyclability

A. De Adhikari (✉)
Department of Chemical Engineering, Indian Institute of Technology Kanpur, Kanpur 208016, India
e-mail: amritainsp.02@gmail.com

S. K. Tiwari et al. (eds.), *Biomass-Based Functional Carbon Nanostructures for Supercapacitors*, Green Energy and Technology,
https://doi.org/10.1007/978-981-99-0996-4_9

1 Introduction

Carbon exists in various forms and allotropes, including mesoporous carbon, fullerenes, graphene, carbon nanotubes, and their composites. [1–3] Each form possesses certain advantages and disadvantages; therefore, the development of their nanostructures can be very challenging and also interesting. Low-cost carbon materials have always been a top priority for industries, as long as economy and profits are considered. Such carbon-based materials have a wide range of applications, but here in this chapter, we shall deal with their supercapacitor (SC) applications. SCs are well-known and extensively researched energy storage systems with a high power density and a long cycle life that aid in renewable energy generation [4]. The deciding parameters for making an SC work efficiently are significantly dependent on the electrode materials. The electrode material that can host facile electrostatic interactions, electron transfers, and good adsorption sites is suitable for SCs applications [5, 6]. Therefore, carbon-based electrode materials have gained attention for their practical and convenient application. Biomass can be an excellent precursor for carbon electrodes. Abundant agricultural residues are produced that can be processed and used for the synthesis of electrode materials. A variety of biomass-based carbonaceous materials have been obtained from different biomass sources, as shown in Table 1. Hydrothermal carbonization (HTC), chemical activation, and pyrolysis are some of the thermochemical treatments carried out in order to obtain porous, high-surface-area products, which are crucial for SCs'application [7].

Also, various studies have shown that carbon materials can indorse in the core-shell nanostructure formation by capturing metal or metal oxide if they are present during the carbonization process. [9, 10] Carbonaceous materials used solely for SCs applications have drawbacks such as low electrical conductivity, poor permittivity, poor polarization ability, and so on [11]. Incorporation of metal/metal oxide species or redox active species (MnO_2, RuO_2, V_2O_5, SnO_2, ZnO, conducting polymers, etc.) influences the energy storage performance at the interface of electrodes and electrolytes [12–19]. Such redox active species are known as the pseudocapacitors in SCs, which can store charge through the transfer of electrons via reversible redox reactions. The carbonaceous materials, on the other hand, store charge via an electrochemical double-layer mechanism (EDLC). Therefore, metal doping or heteroatom doping can improve the electrochemical properties of the SCs device via the synergistic effect between the pseudocapacitors and EDLC materials [20]. This chapter will deal with the physicochemical and electrochemical performance of biomass-based metal-doped electrode materials, which aid in cyclic stability valuation and sustainable routes to the bioeconomy.

Table 1 Some biomass sources and their method of activation for deriving carbon frameworks [8]

Biomass source	Activation
Banana peel	$Zn(NO_3)_2$
Rice husk	$ZnCl_2$
Sugarcane bagasse	$ZnCl_2$
Bamboo	KOH
Seaweed	Thermal
Willow catkins	KOH
Soybeans	KOH
Pomelo peel	KOH
Sunflower seed	KOH
Waxberry	$Fe_2(SO_4)_3$
Perilla frutescens leaf	Thermal
Paulownia sawdust	NaOH
Lessonia nigrescens	Thermal
Celtuce leaves	KOH
Kelp	Thermal
Corn and protein	KOH
Lignosulfonate	Thermal
Auricularia	Thermal
Cassava peel waste	KOH+CO_2
Argan seed shells	KOH

2 Overview

Reduced consumption of fossil fuels and the goal of establishing a low carbon cycle are global necessities for long-term growth. The development of renewable and clean sources of energy is one of the most efficient solutions to reaching this target. This chapter highlights the biomass-derived electrode materials that primarily aim to improve the electrochemical performance and cyclic stability of the electroactive materials. Designing various biomass-derived carbonaceous skeletons from 1D to 3D can become a diverse method to obtain interconnected porous structures. Incorporation of metals or metal oxides contributes to the pseudocapacitance of the electrode material by maximizing the electroactive sites, packing density, and overall capacitance. By adjusting the pore structure, density, doping, electrolyte, and surface area of the biomass-derived carbon, the low volumetric performance can be overcome. Looking into the existing challenges, the scientific community performs in-situ techniques to monitor the functionalization of the biomass-derived carbon that can pave the way from fundamental to operational chemistry. This script can provide a good guideline for designing the next-generation electrode materials for energy storage applications.

3 Cyclic Stability-A Crucial Parameter for SCs Performance

The retention of capacitance of electroactive materials under certain test conditions or after a certain number of charge-discharge cycles is referred to as cyclic stability. Cyclic stability is highly influenced by the type of electrode materials and their process of energy storage. The EDLCs' electrode materials, like carbon materials, are found to belong to type I cyclic stability, where there is no change of phase during charge-discharge cycles and no chemical charge transfer reactions take place in the electrode material. Here, the charge is stored via a reversible adsorption-desorption process at the electrode-electrolyte interface. Thus, there is very little decay of capacitance during many cycles of charge-discharge, and the retention rate is nearly 100%. Such cyclic stability is classified as type I. The second class of cyclic stability is type II, which is generally observed in the case of pseudocapacitive materials (metal/metal oxides, hydroxides, nitrides, carbides, etc.) or battery-type materials, where the charge storage mechanism is via surface-controlled faradic redox reactions. At the initial stages of charge-discharge cycles, there is self-activation of the electrode material, so there is an increase in specific capacitance over the initial value and the retention is always above 100%. After the self-activation step, the rate of retention drops to the initial capacitance or less than 100%; this type is classified as type II. Type III cyclic stability is mostly observed in conducting polymers. In the polymer matrix, rapid, reversible P and N type doping and counter-doping reactions occur. The conducting polymers easily collapse during the charge-discharge process, showing capacitance retention below 100%. The key prompting aspects of cyclic stability include the potential window, electrode materials, scan rate, current density, mass loading, composition of electrolyte, etc.

4 Factors Influencing the Cyclic Stability

4.1 Structural Features of Nanostructured Electrode Materials Derived from Biomass

Tailoring the porosity, geometry, and composition of the biomass-derived nanostructures can lead to enhanced electrochemical performance. There are various methods of synthesizing carbon nanostructures derived from biomass, as noted in Table 1. High specific surface area, heteroatom doping, and high porous structures are some of the interesting traits in regard to increased conductivity and specific capacitance .

4.1.1 High Specific Surface Area

The EDLC mechanism takes place effectively when the carbonaceous electrode materials provide a high specific surface area, leading to better ion adsorption at the electrode/electrolyte interface—a prerequisite for optimizing the specific capacitance [21, 22]. The pore structures and their distribution throughout the architecture greatly influence the electron and ion movements, affecting the electrochemical behavior of the electrode materials. Several crucial parameters of SCs, like power density, energy density, etc., can be improved by optimizing the pore size distribution that is beneficial for the ion transport phenomenon [23]. In aqueous and organic electrolytes, microporous structures (2 nm) with pore sizes of 0.7 and 0.8 nm, respectively, were found to be operative sizes for ion accumulation, confirming high specific capacitance [24]. One of the most versatile procedures to obtain microporous carbons is KOH-assisted pyrolysis, where the reaction between carbon and potassium compounds leads to the production of gases due to the gasification of carbon. Such gasification can create multiple pores within the carbon structure, which are created by washing away the intercalated K^+ ions. [25] CO_2 activation is an alternative approach for the production of microporous carbon at high temperatures, which generates active ion storage and pathways for mass diffusion [26, 27]. Mesoporous (2–50 nm) structures also provide fast transport of ions, leading to higher power densities and rate capacities. Steam activation and ZnCl2 salt activation are some of the methods used to produce mesoporous structures with a mean pore size of 3.2 nm [28]. Elongated time of activation and flow rate of water increase the number of mesopores. ZnCl2 salt acts as a hard template and activating agent to produce mesopores [29]. Macroporous (> 50 nm) structures are large reservoirs of ion-buffering, minimizing the distance of ion diffusion. Micro-and mesoporous structures offer a high specific surface area for accommodation of ions, whereas mesoporous and macroporous structures result in channels for mass diffusion and ion transport [30, 31]. Therefore, it has been observed that pores offer channels for ion transport, ion-buffering spaces, and ion adsorption. However, there is no linear relationship between high surface area and enhanced capacitance. The very small pore size of the micropores restricts the full accessibility of the electrolytic ions, reducing the power and energy density. Again, the ultrahigh pore size of the macro and meso pores causes low packing density, reducing the volumetric capacitance and the electrical conductivity [32]. Thus, the overall architecture with optimal pore sizes, packing density, and sufficient transport channels contributes to the enhanced electrochemical performance [32, 33].

4.1.2 Heteroatom Doping

The doping of heteroatoms within the carbon structure improves the electrical conductivity and wettability. Also, the redox reactions taking place because of the presence of the functional groups at the surface lead to a pseudocapacitance contribution [34, 35]. Biomass-derived nanostructures can be doped with heteroatoms by using precursors enriched with heteroatoms and chemical dopants that can modify

the electronic properties and the surface chemistry [36]. For instance, N doping can provide electroactive sites, improve wettability, and increase electrical conductivity, thereby enhancing the electrochemical activity [37]. The pyridinic and pyrrolic-N atoms have negative charges and provide pseudocapacitance, whereas the pyridinic-N oxide and quarternary-N atoms have a positively charged atom that facilitates electron transfer. Some of the N containing raw biomass includes silk, fish skin, soybean, tree bark, shrimp shell, bamboo shoot, egg white, gelatin, etc [38–45]. The addition of O as a heteroatom has also been found to improve electrochemical performance. O functionalities behaving as electron acceptors improve the wettability of the electrode, increase ion accessibility, and provide pseudocapacitance through redox reactions. O doping can be realized by using O-rich precursors or a suitable activation method like KOH, air, or acid [46–48]. S-doping on the surface of a carbonaceous material acts as an active site for redox reactions and improves wettability [49–51]. S contains one lone pair of electrons on the p-orbital, which overlaps with the p-orbital of the sp2 hybridized graphite; such interaction results in delocalization of electrons within the carbon backbone [52]. S-containing thiourea and thioglycolic acid are good sources of sulfur. Also, the S-doped carbons have low charge transfer resistance owing to the better polarity on the surface of the carbon. Electrochemical properties also depend on the doping degrees and dopant arrangements. However, the mechanism by which the doping effect affects the electrochemical properties still remains unclear.

4.1.3 Hierarchical Nanostructures

Nanostructures derived from biomass show different dimensions of architectures from 1 to 3D, i.e., nanofibers, nanosheets, etc. Such well-defined structures offer high porosity, a specific surface area, and conductivity—all necessary for rapid ion transport leading to high electrochemical performance. 1D nanobelts, nanofibers, nanothreads, etc. have conductive channels for the transport of electrons with exceptional mechanical strength [53–56]. A 1D skeleton enables the migration of ions from bulk electrolytes to interior pores, which is favorable for high rate performance. One of the widely used techniques to produce 1D nanofiber is electrospinning. Controlling the heating rate at the time of carbonization allows the morphologies of the products to be tuned. Cotton and polar catkins are examples of biomass that can be directly converted to 1D fibers due to their tubular structure [57, 58]. Such tubular morphology acts as conductive channels for the rapid transport of ions. Further, the hollow scaffolds of the carbon architecture also act as ion transport and buffering sites, making them beneficial for the high rate capability. Also, the higher length/diameter ratio of the porous nanostructures shortens the diffusion path and offers high surface ion charge storage. 2D nanosheet structures deliver large surface contact areas, good conductivity, and low resistance. [59] But the nanosheets have the possibility of stacking between their adjacent layers, reducing the ion transport and rate capabilities [44, 60]. 3D porous architectures derived from biomass possess less internal resistance, shorter ion diffusion paths, and increased charge transfer kinetics as they

have a large number of pores, a highly interconnected morphology, and good mechanical stability. The 3D honeycomb design hosts the ions and reduces the ion diffusion resistance, resulting in favorable electrochemical performances.

There are also certain inherent biomass nanostructures that possess porous morphology, aiding tunable electrochemical properties. For example, some wood-based carbonaceous materials have vertically allied multi-channels for the transport of ions, which reduce tortuosity, contributing to high rate capability [61]. The interspace between the pores facilitates ion transport and enhances the specific capacitance. There are some inherent free-standing electrodes, like the flat flower petal, whose wrinkled morphology, high conductivity, and 5–10 m thickness make them suitable as self-standing electrodes for flexible SCs. There are also certain biomass-derived electrodes that can be employed as binder-free flexible electrodes, like flax fabric-derived carbon, obtained via facile carbonization [62] (Table 2).

Table 2 Different methods of synthesis of biomass-derived carbon structures and their special features [63]

Method of synthesis			Temperature range	Special features
Pyrolysis	Gas assisted	Air	<500 °C	Incorporation of oxygen functional groups with inherent morphology.
		Steam, CO_2	600–1200°C	Large surface area porous structures
	Self-activated	Physical or chemical activation	600–1700°C	Eco-friendly strategy as no external activating agent is required
	Chemical assisted	NaOH, KOH, H_3PO_4, $CaCl_2$, $ZnCl_2$, $FeCl_3$	400–1000°C	Most commonly used method of activation employing hard templates and activating agents.
Template methods	Soft template	Polymers		Well organized structure obtained with hierarchical morphology with adjustable porosity.
	Hard template	Metal oxides, silica, molten salts		
Hydrothermal carbonization	Graphene oxide assisted		<250°C, followed by carbonization at high temperature	Well-designed architecture porous morphology.

4.1.4 1D Biomass-Derived Carbon Materials

1D fibrous structure possesses various advantages as follows:

(a) It has very good mechanical properties with high strength of 2−3 GPa and Young's modulus of 138 GPa [64–66].
(b) On chemically modifying the surface of the 1D fibers, the surface active sites are created that can improve the electrochemical properties [67–69].
(c) Fibrous geometries have high aspect ratio and can form interconnected binder-free networks for flexible SCs [70, 71].
(d) The linear 1D channel is capable of providing pathways for facile transfer of electrons and ions [72].
(e) The tubular structure can act as a buffer reservoir for the electrolytes offering more active sites for electrochemical reactions [73].

The various 1D biomass-derived precursors include willow catkins, kapok, cotton, flax, bacterial cellulose, ramie, etc [74–79]. Zhang et. al. synthesized MnO_2/carbon microtube bundle composite for SCs electrodes [80]. The carbon microtube was produced from sawdust and MnO_2 nanostructures were obtained by anodic electrodeposition. The deposition of MnO_2 increases the active sites and also the conductivity of the electrode material. The composite offered a specific capacitance of 617.6 F/g at 1 A/g and cyclic stability was tested over 1000 cycles. The electrochemical studies showed that it exhibited very low resistance, high charge storage ability, and good transfer capability. In this study, the researchers exploited the natural tubular features of the existing woods and enhanced their electrochemical performance. Zhang et al. used willow catkins as a precursor to synthesize porous graphitic carbon nanotubes (PGCMT), which acted as a substrate for electrodeposition of MnO_2 [81]. The PGCMT/MnO_2 composite showed excellent specific capacitance of 550.8 F/g at 2 A/g with 89.6% cyclic stability after 5000 cycles. Xu et al. fabricated micro-tubular carbonized kapok fiber/NiO nanocomposites for SCs application [82]. The hollow tubular kapok fibers are used as templates to grow $Ni(OH)_2$ via hydrothermal process, then converted to NiO via carbonization. The composite so prepared has very good supercapacitive properties with specific capacitance of 575.5 F/g at 0.5 A/g with a capacitance retention of 91.7%. Asymmetric SCs device assembled out of this composite has an energy density of 7.5 Wh/Kg and power density of 65.5 W/Kg.

The above discussions highlight some of the fantastic features and electrochemical properties of 1D biomass-derived metal composites along with low cost fabrication and fast charge-discharge rates.

4.1.5 2D Biomass-Derived Carbon Materials

2D nanostructured biomass has great prospective and the following features are essential for electrochemical energy storage:

(a) The 2D structure has strong in-plane covalent bonds and also high conductivity that can speed up the electrons flow [83, 84].
(b) The 2D layered structure has an ultrathin dimension with large lateral size reducing the ion transport path [85, 86].
(c) Open and flat surface exposes the surface active sites, enhancing the surface area for better exchange of ions at the electrode-electrolyte interface [87].
(d) 2D structures have active edges and in-plane defect sites that can facilitate the storage of charges and high specific capacitance [88].

Different precursors of the 2D biomass-derived carbonaceous materials includes silk, Perilla frutescent, bougainvillea flowers, eggplants, puffed rice, etc [38, 89–92]. These precursors intrinsically possess multiple layered structures and rearranges to form 2D sheets on pyrolysis.

4.1.6 3D Biomass-Derived Carbon Materials

3D nanostructures having salient properties that are beneficial for SCs application are:

(a) Increasing the dimensionality, increases the active surface area, therefore improving the supercapacitive performance of the materials.
(b) The 3D microstructures are interconnected with wide range of pores that can provide facile transfer of ions and good electrical conductivity.
(c) They can be tailored into novel structures beneficial for high electrochemical performance.

The assimilated properties, therefore, offer high power delivery and high energy storage with short ion path. For instance, Song et al. studied 3D carbon hierarchical porous structures, synthesized from corn husks via direct pyrolysis of KOH. The internetwork macroporous morphology was obtained because of the inherent cellular architecture of cellulose. Narrow pore size distribution, rich doping of oxygen, and synergistic effect enhances the supercapacitive performance. The specific capacitance obtained was 356 F/g with a rate capability of 84.3% and cyclic stability of 95% over 2500 cycles [93]. Yang et al. synthesized 3D honeycomb porous carbon from pomelo peels via carbonization further by KOH activation [94]. The interconnected honeycomb architecture has high surface area of 2725 m^2/g, efficient for electrolyte diffusion. This was then doped with N which further enhanced the electrochemical performance. The material exhibited a specific capacitance of 342 F/g and volumetric capacitance of 171F/cm^3 at 0.2 A/g. It showed a rate capability of 62% and cyclic stability of 98% over 1000 cycles. Zhao et al. synthesized HPCs from ant powder, in which the exoskeleton of ant contains chitin, facilitating 3D frameworks [95]. Furthermore, the exoskeleton is a rich source of fatty acid and protein, therefore the carbon framework contains many heteroatoms doped skeleton. The ant powder also has many metal salts, making it a natural porous template structure. The obtained biomass possesses high surface area of 2650 m^2/g with suitable pore

sizes. Such morphology enhanced the electrochemical performance of the material with a specific capacity of 352 F/g at 0.1 A/g, high retention rate of 80%, and cyclic stability after 10000 cycles.

4.2 Metal Doping of Biomass-Derived Nanostructures

Metal/metal oxides or hydroxides are often incorporated within the carbon structures in order to contribute to the pseudocapacitive behavior. The typical redox reactions of these materials results in adsorption of ions at the electrode-electrolyte interface and enhances the energy density of the SCs. The sole use of these metal derivatives is restricted because of their low specific surface area, structural instability, and low intrinsic conductivity. But doping of metals within the biomass-derived nanostructures, offers suitable space for the electroactive sites where the redox reactions can take place. The porous structures of the carbon skeleton can promote charge transfer, leading to high energy density and rate performance. Also, the robust biomass architectures are resistant to mechanical stress caused by the faradic reactions and thereby increase the cyclic stability of the hybrids. Therefore, metal-doped biomass-derived structures enhances capacitance, energy density, rate performance, and cyclic stability. The following section will elaborate on some of the metal/metal oxides or hydroxides that have been incorporated within the biomass to enhance the electrochemical performance.

4.2.1 Nickel/Nickel Oxide or Hydroxide Biomass-Derived Nanostructures

Nickel and its derivatives have been regarded as electroactive materials for the SCs application. They have diverse morphologies, easy synthesis, and rapid redox reaction kinetics [96]. They have good synergism with the carbon frameworks as a result provide better electrochemical properties. Li et al. reported the deposition of β-$Ni(OH)_2$ nanosheets within the carbon microtubes derived from catkins via hydrothermal carbonization technique [96]. The willow catkins are biomass precursors having 1D hollow tube structures with a diameter ranging from $6-10\mu m$. They are known to have good capillarity, facilitating transport of nutrients and moisture. It is used as a bio-template to produce hollow carbon microtubes to support active nanomaterials. The porous hollow microtube acted as conductive channel for charge and ion transport and the morphology is regulated and controlled by adjusting the amount of $Ni(NO_3)_2.6H_2O$. The high pseudocapacitance of β-$Ni(OH)_2$ results in high energy density of 37.8 Wh/Kg. The β-$Ni(OH)_2$- catkins derived microtube offered a specific capacitance of 1568 F/g at 1 A/g with a retention of 51% capacitance at 20 A/g and excellent cyclic stability of 84.3% after 3000 cycles. Cao and co-workers derived biochar from waste biomass and then subjected it to Ni sorption. The Ni adsorbed biochar was then employed for supercapacitor application via microwave

treatment [97]. The capacitance was found to be higher in case of microwave assisted Ni-biochar compared to without microwave activation. This enhancement can be attributed to the formation of NiO and NiOOH species from Ni(II). It also exhibited high stability after 1000 cycles with less than 2% loss. This work showed a conjugation of conservation of environment and also storage of energy.

Zhang et al. reported Ni in-situ doping to obtain cellulose based N/Ni co-doped porous carbon [98]. The microcellulose assembly under hydrothermal treatment led to the generation of honeycomb architecture facilitating the uniform distribution of N and Ni within the interconnected networks. The pore size of the porous carbon ranged between 1.7−4 nm, which is beneficial for better ion mobility and adsorption site. The resulting Ni-doped electrode material delivered a specific capacitance of 415 F/g at 0.5 A/g with capacitance retention of 72.22% at 20A/g. The cyclic stability was tested upto 10000 cycles showing a retention rate of 87.87%. They also observed that one-pot hydrothermal treatment strategy to incorporate Ni and N was beneficial for increasing the energy density and cycle life of the electrode material. Zhu and co-workers developed biomass-derived sustainable C/N–$Ni(OH)_2$/Ni_xS_y electrode material having a sandwich structure [99]. The biomass precursor used was egg white, owing to its natural abundance, good sources of N and C, as a source of S to form Ni_xS_y. The doping improves the electrical conductivity and increases the active sites for redox reactions. Ni_xS_y are dispersed and anchored on $Ni(OH)_2$ nanoflakes giving a flake/particle sandwich structure. The electrode material exhibited a specific capacitance of 1731.2 F/g at 0.5 A/g and a hybrid SCs constructed out of this shows an excellent cyclic stability of 107.6% upto 10000 cycles. Fu et al. reported $Ni(OH)_2$/sorghum stalk biomass composite obtained via microwave treatmentx [100]. Herein, biomass was first derived from sorghum stalk and $Ni(OH)_2$ was deposited on it via microwave method of deposition. The electrode material exhibited a specific capacitance of 889.2 F/g at 2A/g and capacitance retention of 95.9% over 30000 cycles. The microwave deposition assisted the uniform growth of $Ni(OH)_2$ on the sorghum stalk, resulting in enhanced electrochemical performance (Fig. 1).

4.2.2 Cobalt/Cobalt Oxide or Hydroxide Biomass-Derived Nanostructures

Cobalt or its oxides and hydroxides have been widely exploited for energy storage applications. On incorporation of cobalt and its derivatives within the porous biomass-derived skeleton, the electroactive spots are increased also increasing the cyclic stability of the system [101]. Madhu et al. reported the synthesis of activated carbon derived from Pongam seed shells and made a composite out of it with cobalt oxide [102]. The nanocomposite PSAC/Co_3O_4 showed a small transfer resistance owing to the synergism between Co_3O_4 and PSAC. Shi et al. studied the sandwich Co_3O_4@carbon fiber@Co_3O_4 for SCs application [75]. The porous hollow structure offers high specific capacitance of 892 F/g at 0.5 A/g with a long cyclic stability of

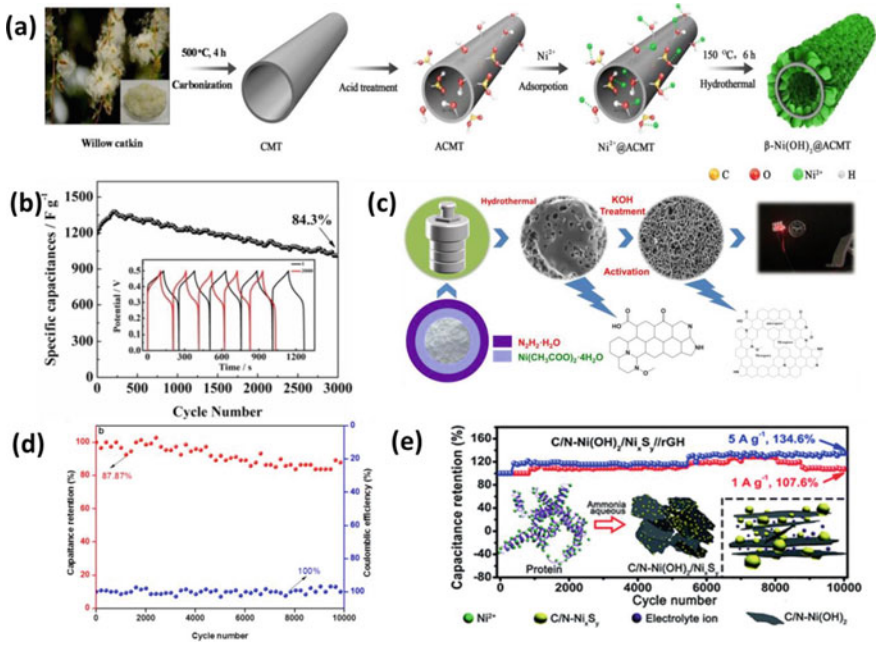

Fig. 1 Some reported nickel/nickel oxide or hydroxide biomass-derived nanostructures. **a**, **b** Scheme showing the synthesis of β-Ni(OH)$_2$@AMCT composite and the cyclic stability of the composite [96]. **c**, **d** Synthesis scheme of cellulose based N/Ni co-doped porous carbon and cyclic stability [98]. **e** C/N–Ni(OH)$_2$/Ni$_x$S$_y$ electrode material and its cyclic stability upto 10000 cycles [99]. (All figures are reprinted with permission)

88% over 6000 cycles. The hollow structure provides inner wall space to accommodate the Co_3O_4 particles and therefore enhances the redox reaction sites and serves as promising electrode material. Ouyang et al. synthesized NiCo-LDHs/BPC porous composite for supercapacitor application [103]. They observed that composite electrode material offered a high specific capacitance of 2047 F/g at a current density of 1 A/g, suggesting good interaction between BPC and LDH. Asymmetric SCs were also assembled where the composite was employed as the cathode, where the SCs delivered a capacitance of 139 F/g at 1 A/g with a cyclic stability of 75.8% after 6000 cycles. The composites were synthesized via single step solvothermal process, where NiCo-LDHs were deposited over the biomass-derived porous carbon, and arrays of nanosheets were assembled to give a spherical structure. Such hierarchical structures possess many electroactive sites facilitating ion transport and diffusion. Another such study of NiCo-LDHs nanosheets for SCs application was reported by Wang et al., where, in-situ growth of NiCo-LDHs was carried out on porous carbon derived from Dicranopteris dichotoma [104]. The synthesis of such a structure avoids the complicated growth process, induces nucleation and controllable growth, and promotes charge transfer ability and rate capability. The special structural features of LDHs nanosheets, like its dimension (6.20 nm), high surface area,

high wettability, and low charge transfer resistance also merits the electrochemical performance of the SCs. A hybrid SCs constructed out of it offers a high energy and power density of 52.47 Wh/Kg and 375 W/Kg respectively, with high capacitance retention of 75.9% after 4000 cycles. Qu et al. reported NiCo-LDH nanosheets regulated by carbon dots derived from fungus bran to form 3D flower-like morphology [105]. The role of carbon dots are ascribed to the formation of 3D spheres from 2D spheres, having more electroactive sites. The optimized obtained electrode material exhibited fair electrochemical performance with a specific capacitance of 2100 F/g at 1 A/g. Asymmetric SCs device was assembled which also delivered a high energy density of 52.5 Wh/Kg at a power density of 750 W/Kg, it can maintain 80% of its initial capacitance upto 5000 cycles. Zhang et al. reported for the first time, SCs devices assembled with metal silicates. They reported the preparation of bamboo leaves derived porous carbon along with Ni-Co silicate as cathode material for SCs [106]. The Co-Ni silicate attains a sheet petal-like structure, offering a specific capacitance of 368 F/g at 0.5 A/g and cyclic stability of 89% upto 10000 cycles. The authors claimed that their work can offer a potential pathway for the synthesis of metal silicates to recycle silicon enriched biomass and synthesize some useful materials (Fig. 2).

4.2.3 Manganese/Manganese Oxide Biomass-Derived Nanostructure

Manganese dioxide has been found to be a very good pseudocapacitive material owing to its high theoretical capacitance of 1370 F/g. The pseudocapacitance arises from the faradic reaction between Mn^{4+} and Mn^{3+} at the interface. A lot of porous carbon skeleton has been employed to grow MnO_2 and its derivatives in order to overcome the low intrinsic conductivity of manganese [107–110]. Wang et al. derived porous carbon from enteromorpha prolifera (ACEP), which acted as a template to grow MnO_2 nanostructure by wet chemical process [110]. The anchoring of the δ-MnO_2 nanosheets were optimized by modulating the reaction time. The ACEP@δ-MnO_2 electrode showed a high specific capacitance of 345.1 F/g at 0.5 A/g with cyclic stability of 92.8% after 5000 cycles and when assembled as a positive electrode in asymmetric SCs, offered a high energy and power density of 31.0 Wh/Kg and 500 W/Kg respectively. Yang et al. reported vertically grown MnO_2 on the surface of the hemp derived porous carbon (HC) [111]. The MnO_2/HC composite was synthesized via one step hydrothermal process, which produced 3D architecture with interconnected network. The porous HC acts as an ideal host to anchor the MnO_2 offering high pseudocapacitance with better ion and electron transport. The composite delivered a specific capacitance of 340 F/g at 1 A/g with rate capability of 88%. Asymmetric SCs were constructed with MnO_2/HC as the positive electrode, which showed an energy density of 33.3 Wh/Kg and power density of 14.8kW/Kg. Gogoi et al. obtained coconut derived porous carbon with $MnCo_2O_4$ nanorods and MnO_2 nanoscales supported on it [112]. The MCO-MnO_2-PC so obtained delivered a specific capacitance of 1330 F/g at 3 A/g and was employed as a positive electrode in flexible asymmetric SCs. The asymmetric device showed a power density of 1600

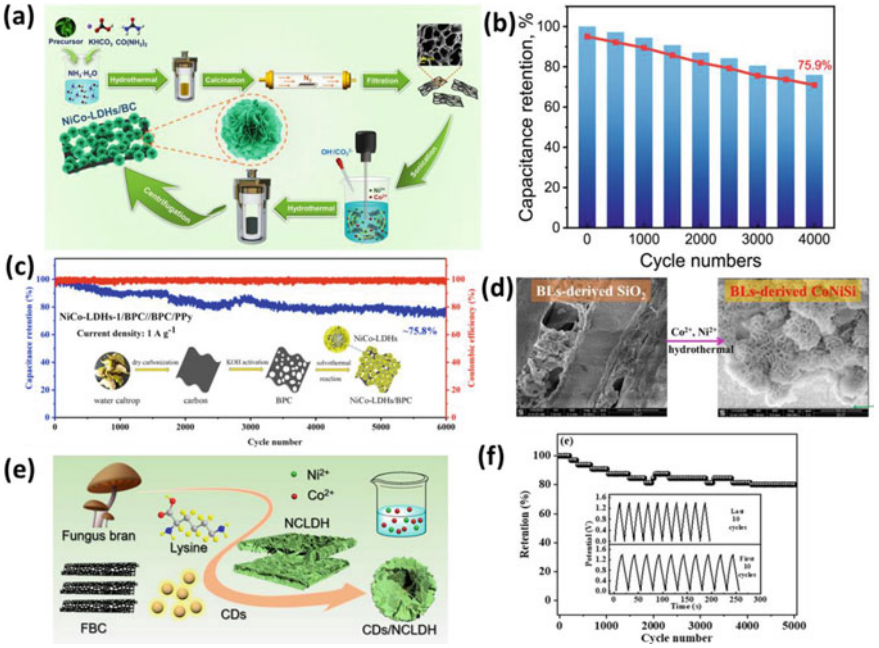

Fig. 2 Some reported cobalt/cobalt oxide or hydroxide biomass-derived nanostructures. **a** Scheme showing in-situ growth of NiCo-LDHs on porous carbon derived from Dicranopteris dichotoma and **b** the cyclic stability of the electrode material [104]. **c** Synthesis and cyclic stability of NiCo-LDHs/BPC porous composite for supercapacitor application [103]. **d** Bamboo leaves derived porous carbon along with Ni-Co silicate as cathode material for SCs [106]. **e** NiCo-LDH nanosheets regulated by carbon dots derived from fungus bran to form 3D flower-like morphology and **f** cyclic stability of the supercapacitor constructed with it [105]. (All figures are reprinted with permission)

W/Kg and energy density of 81.3 Wh/Kg, long shelf life, high rate capability, and cyclic stability of 92% upto 5000 cycles. The PC acts as a solid support for accommodating the MnO_2 and $MnCo_2O_$, providing a shorter ion travel path for the ions with enhanced electrochemical performance. Wang et al. derived porous carbon (EC) by carbonizing the eggplant skin and made a composite with MnO_2 (MnO_2/EC) via hydrothermal method [113]. The composite showed a morphology where the urchin shaped MnO_2 was decorated on the folds of EC surface. The presence of MnO_2 offered pseudocapacitance to the system, enhancing the overall capacitive performance with a specific capacitance of 652.5 F/g at 0.5 A/g and cyclic stability of 79.2% after 10000 cycles. Ganesh et al. studied the low temperature solution process for growing MnO_2 nanorods anchored on carbon framework derived from sweet potato [114]. MnO_2@C composite showed a specific capacitance of 718 F/g at 2 mA/g and a cyclic stability of 89% after 5000 cycles. Mofrad et al. showed the synthesis of carbonaceous aerogel (CA) from watermelon and the Fc-modified MnO_2 obtained by solvothermal route was physically mixed with CA in acetone to obtain MnO_2-Fc/CA [115]. The authors claimed that they synthesized battery-type

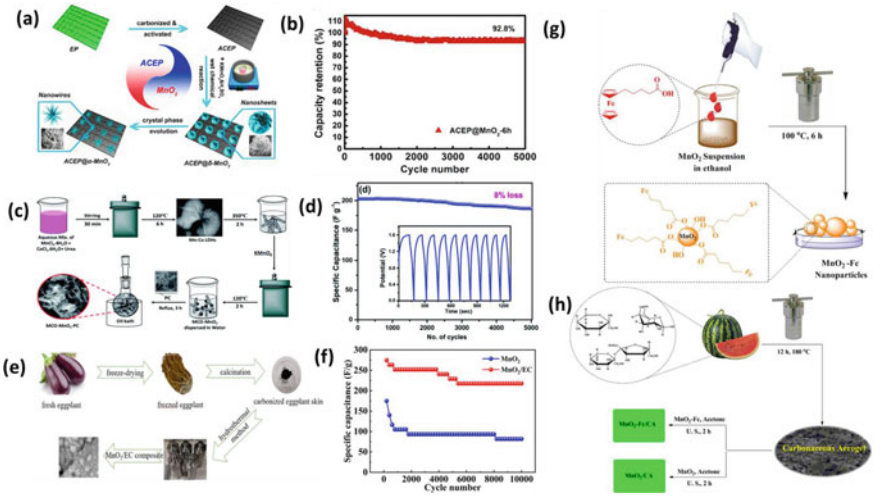

Fig. 3 Some reported Manganese/ manganese oxide biomass-derived nanostructures. **a** MnO_2 nanostructures grown on porous carbon derived from enteromorpha prolifera (ACEP) and **b** Cyclic stability of the electrode material [110]. **c** Synthesis of $MnCo_2O_4$ nanorods and MnO_2 nanoscales decorated on porous carbon derived from coconut composite (MCO-MnO_2-PC) and **d** Its cyclic stability [112]. **e** MnO_2/EC composite synthesized via hydrothermal method using eggplant and **f** Cyclic stability of the material [113]. **g** Synthesis of Fc-modified MnO_2 nanoparticles obtained by solvothermal route. **h** Fc-modified MnO_2 nanoparticles were physically mixed with carbonaceous aerogel (CA) (obtained from watermelon) in acetone to obtain MnO_2-Fc/CA [115]. (All figures are reprinted with permission)

electrode material, where Fc functions as electroactive material on the surface of MnO_2. The nanocomposite delivered a specific capacitance of 963 F/g at 1 A/g with an excellent cyclic stability of 96% after 3000 cycles. A symmetric cell assembled with this electrode material offered a power density of 4556 W/Kg and energy density of 38.1 Wh/Kg (Fig. 3).

4.2.4 Copper/Copper Oxide or Its Other Derivatives Based Biomass-Derived Nanostructure

Copper oxide possesses high chemical stability, ease of availability and environment compatibility, and high theoretical capacitance [116, 117]. Research by various groups has shown that the electrical conductivity of the carbonaceous materials can be enhanced by incorporation of Cu and its derivatives [118–120]. Hu et al. synthesized porous carbon from walnut shell and modified it with Cu/Cu_2O [121] The synthesized material was used as SCs electrode material that delivered a specific capacitance of 360 F/g at 0.5 A/g which offered a cyclic stability of 81.8% after 6000 cycles. Verma and co-workers synthesized PA/AC/CuF as an electrode material for SCs application [122]. In this work, the activated carbon (AC) was derived from coconut shell

via pyrolysis. The fabricated electrode material showed a specific capacitance of 248.3 F/g, energy density of 49.66 Wh/Kg, and power density of 5996.6 W/Kg. The cyclic stability was observed to be 92.8% after 2500 cycles. Copper ferrite (CuF) are somewhat less explored material for SCs application, therefore this work is an example to research such material in future. CuF has diverse oxidation states owing to the presence of Cu^{2+} and Fe^{3+} ions, thus providing bulk redox reactions at the surface and high charge storage ability. Sun et al. reported a new electrode material, 3D bimetallic organic framework/ biomass carbon composite [123]. The carbon was derived from grapefruit peel by carbonization method and then modified with MOF in different ratios. The composite so obtained was employed for SCs application and also for Li ion batteries. The electrochemical performance was obtained best when the doping of carbon was 20% of the active substance.

4.2.5 Iron/Iron Oxide or Its Other derivatives Based Biomass-Derived Nanostructure

Iron oxides or other derivatives of iron are found to be good electrode materials for SCs owing to their natural abundance, low cost, and environment friendly. Iron can undergo reversible redox reactions between Fe^{3+} and Fe^{2+}. Incorporation of iron oxides within the carbonaceous framework improves the conductivity, increases the ionic diffusion, and enhances the cyclic stability of the material [124]. For example, Wu et. al. developed sponge like carbon gels (CGs) from watermelon [125]. To the synthesized gels Fe_3O_4 nanoparticles were incorporated within the carbonaceous network. Fe_3O_4/CGs composite was then transformed into magnetite aerogels via calcination. This aerogel has good conductivity and porous morphology and therefore depicted excellent capacitive behavior with a specific capacitance of 333.1 F/g at 1 A/g and excellent cyclic stability of 96% after 1000 cycles. Zhang et al. studied a simple process to encapsulate nanoparticles of iron into N, P co-doped biomass-derived carbon nanotubes [126]. The precursor used for biomass was egg yolk, which is a rich source of heteroatom. The synthesized electrode material has a very high surface area to accommodate the ions, offering a high pseudocapacitance. A symmetric SCs assembled with this electrode material exhibited a specific capacitance of 392 F/g at 0.5 A/g with a long cyclic stability over 50000 cycles. Butnoi et al. prepared a composite out of lignin based fibers with iron oxide nanoparticles (L-CNFs@Fe_xO_y nanofibers) by electrospinning [127]. Lignin based fibers can be easily obtained at low cost and also the electrospun technique helps to develop interspaced carbon fibers, advantageous for electrolyte accessibility. The nanostructured composite delivered a high energy density of 43 Wh/Kg, specific capacitance of 216 F/g at 0.1 A/g, and power density of 242 W/kg. 97.6% capacitance retention after 1000 cycles also makes it a potential candidate for the SCs. Venkateswarlu et al. synthesized 2D crumbled porous carbon from waste garlic husk and then composite with Fe_3O_4 nanoassemblies were obtained [128]. Fe_3O_4 nanocrystals undergo nucleation in presence of 2D carbon framework and develop a cluster depicting a pomegranate. The crumbled architecture prevents the agglomeration and restacking of the Fe_3O_4

nanoassemblies, enabling excellent ion diffusion within the porous channels. The Fe_3O_4 NAs@2D-CCS composite depicted a power density of 3000−8000 W/Kg, specific capacitance of 820 F/g at 0.5 A/g, and energy density of 115.5−65.9 Wh/Kg with cyclic stability of 90.1% after 2000 cycles.

4.2.6 Transition Metal Dichalocogenides (TMDCs) Based Biomass-Derived Nanostructure

TMDCs are a class of 2D layered inorganic species having a layer of transition metal between two chalcogen layers. They have been recently exploited as pseudocapacitive material owing to its sheet-like structure, good conductivity, and large surface area [129]. Islam et al. studied the electrochemical properties of MoS_2 nanosheets vertically oriented on plasma pyrolyzed cellulose filter paper [130]. Free standing MoS_2-pCMF electrodes have high surface area because of the vertical arrangement and also increase the electrolyte accessibility. It operates in a wide potential window with a cutoff frequency of 103 Hz at −45° and cyclic stability of upto 50000 cycles. Guo et al. synthesized HMD/rGO/MoS_2 composite using a loofah sponge as the carbon source [131]. Hollow microtubular carbon structure obtained from loofah sponge acts as a template to accommodate MoS_2 nanoparticles (Fig. 4).

4.2.7 MXene Based Biomass-Derived Nanostructure

Transition metal carbides or nitrides are known as the MXenes, which have gained tremendous attention in current times for electrochemical energy storage. This have high packing density, electronic conductivity, and charge storage capacity, making it suitable for SCs application [132]. However, they have a tendency to aggregate and tack between the layers, reducing their effective surface area. Therefore various modifications have been done in order to get electrode materials with enhanced electrochemical performance [133]. Pu et al. synthesized N-doped MXene from chitosan derived from waste seafood for SCs application. [134] Chitosan contains amine and acetamide groups and therefore is a favorable precursor for obtaining N-doped products. N-doped MXene possesses lone pair electrons from N and also the interlayer stacking is avoided owing to doping. The electrode material showed a specific capacitance of 286.28 F/g with 98% efficiency and cyclic stability over 10000 cycles. Sun et al. prepared skin/skeleton MXene/CF porous heterostructure for SCs application [135]. The carbon fibers were derived by direct pyrolysis of the cotton fiber wiper. The MXene nanosheet covers the surface of the CF and bridges the gap between CF and MXene. The interlayer stacking of the MXene gets reduced giving a porous pathway for rapid ion exchange. The MXene/CF electrode material possesses high volumetric capacitance of 7.14 F/cm^3, good rate capability, and cyclic stability of 99.8% after 5000 cycles. Wei et al. decorated $Ti_3C_2T_x$ MXene on porous carbon derived from chitosan. [136]. The sandwiched CPCM/MXene heterostructure has electrostatic interaction with less restacking of the MXene layers that can promote ion

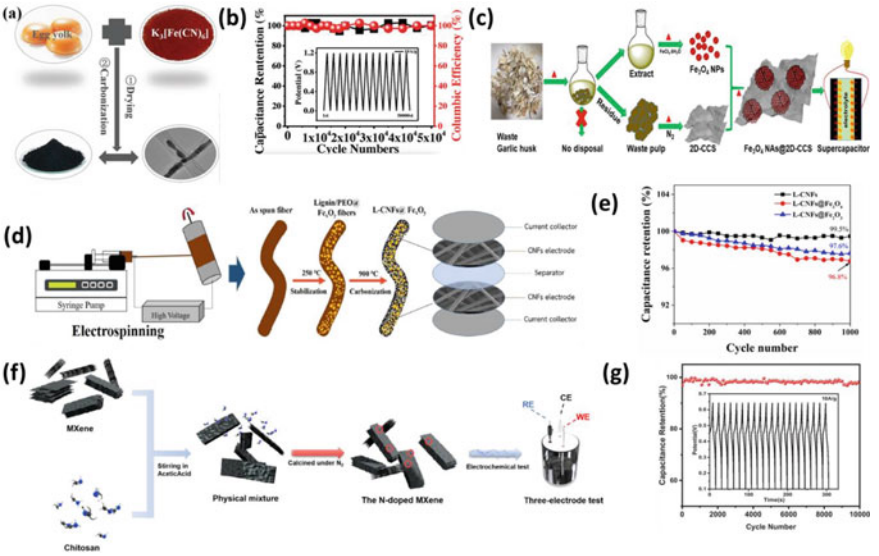

Fig. 4 Some reported iron/iron oxide and MXene based biomass-derived nanostructures. **a** Egg yolk derived biomass iron composite for SCs application and **b** its cyclic stability [126]. **c** Composite made out of 2D crumbled porous carbon from waste garlic husk and Fe_3O_4 nanoassemblies (Fe_3O_4 NAs@2D-CCS) [128]. **d** Lignin based fibers with iron oxide nanoparticles (L-CNFs@Fe_xO_y nanofibers) by electrospinning and **e** its cyclic stability [127]. **f** N-doped MXene from chitosan derived from waste seafood for SCs application and **g** its cyclic stability [134]. (All figures are reprinted with permission)

migration. The good synergism between the components leads to enhanced specific capacitance of 362 F/g at 0.5 A/g, power density 500 W/Kg, energy density 27.8 Wh/Kg, and a cyclic stability of 93.87% after 10000 cycles. Such electrochemical performance provides a new electrode material for SCs application.

4.3 Various Test Parameters

The test parameters like current density, scan rate, and potential window greatly influences the cyclic stability of the electroactive materials. For example, at low current density and scan rate, the specific capacitance is higher while at higher current density and scan rates, capacitance decreases. The reason for such a phenomenon can be explained as, at low scan rates and current density, the ions get enough time to undergo redox reactions and the rate of reactions are equal to the rate of charge transfer. But as the reaction proceeds further, the electroactive material will have a tendency to dissolve or disperse in the electrolyte, thereby decreasing the cyclic stability. However, at some instances, the scan rate and current density are purposefully increased in order to test the cyclic stability. In such cases, only a limited

number of electroactive materials will take part in the electrochemical reactions, and the dissolved materials during the course of the reaction will be replaced by other electroactive materials that are not taking part in the reaction, thereby exhibiting less specific capacitance. Therefore, the testing parameters influence the cyclic stability and must be consistent with cyclic voltammetry and charge-discharge analysis.

5 Challenges and Outlook

This chapter focuses on the recent electrode materials made of biomass-derived carbon and their composites with metal/metal oxide, nitrides, sulfides, etc. Adopting cheap and sustainable raw biomaterial precursors to obtain valued carbonaceous electrodes can reduce the use of non-renewable energy resources. The incorporation of various pseudocapacitive materials within the carbon framework generates rapid redox reactions, high charge transfer, and flexible, stable structures, offering high capacitance and long cyclic stability. However, the biomass-derived carbonaceous materials also face many challenges. For instance, a wide variety of growing environments, harvesting times, and resources of nutrients in the biomass precursor vary at different locations; decay of biomass is very common by insects or animals, etc. All these disadvantages make it difficult to reproduce the electrochemical studies of the materials. Therefore, it is difficult to reproduce the electrochemical properties of carbonaceous materials. Still, taking the economy into consideration, the large-scale use of valuable biomass (e.g., soybean, watermelon, and cocoon silk) for the preparation of porous skeletons outweighs the disadvantages of the biomass-based electrode materials.

The studies have shown that structure modification and biomass activation cannot be separated as both occur simultaneously during the synthesis process. The inherent structural features of the biomass-based materials allow the researchers to perform controlled treatments on them in order to obtain wide, highly porous architectures. The activation step is also found to be an important step for increasing the surface area of the biomass. The prospect of employing a general synthesis process in order to obtain preferred pore structure from a variety of biomass is still a challenge to the scientists. For instance, the molten-salt procedure can be a significant way to control the synthesis of porous structures with variable morphologies [137–140]. Like carbon nanobelts, they were prepared via cutting and stripping techniques in ZnCl2 molten salt, where ZnCl2 acts as a hard template for the generation of pore structure and also acts as a scissor to cut and strip the original materials to obtain the nanobelts [28]. Such carbon materials offer a very high surface area of 1208.0 m2/g and suggest a scalable and controlled approach to achieving biomass-derived carbon heterostructures. Various activation methods, like heteroatom doping, transition metal incorporation, and direct carbonization, have already been explored and employed to build SCs with high volumetric capacitance, but some shortcomings are yet to be met, like low electrical conductivity and bulk density, and weak interaction between carbon and transition metal. Heteroatom doping and pristine

biomass-derived carbon materials possess limited packing density. One such study involved embedding Fe_2O_3/FeS into N,S co-doped carbon material derived from waxberry [93]. The pore morphology was adjusted by controlling the temperature of the hydrothermal reaction and the amount of iron sulfate added. The materials showed very good capacitive performance with a high volumetric capacitance of 1320.4 F/cm^3 at 0.1 A/g, an energy density of 100.9 Wh/Kg, and a power density of 221.9 Wh/L. The material also showed a long cycle life of over 50,000 cycles. Such performance can be attributed to the short diffusion path, porous structure, and multiple heteroatoms due to doping of the carbonaceous skeleton. As a result, the contribution of the pseudocapacitance from the rapid faradic reactions taking place is demonstrated in this work.

A lot of electrolytes have also been investigated in order to obtain a wide potential window for better electrochemical performance. Varieties of electrolytes used are aqueous, non-aqueous, organic, ionic, etc. The operating potential window of an aqueous electrolyte is less than 1 V; non-aqueous electrolytes have a potential window higher than 1.23 V. Ionic liquids and organic electrolytes have a wide potential window of 2.5–4.0 V, making it suitable to obtain SCs with high volumetric energy density, as energy density is proportional to the square of the potential window. However, the electrochemical results obtained with non-aqueous SCs are less than those obtained with aqueous electrolytes, owing to their high viscosity and low ionic conductivity, therefore sacrificing electrochemical performance. The main problem with the non-aqueous SCs is their disparity between the pore structures that are biomass-derived. Still, there have been a lot of challenges with finding the best combination of electrolyte and electrode that can offer better electrochemical properties. It is essential to obtain an in-situ technique of monitoring that can correctly regulate the structural features and charge distribution at the interfaces by properly choosing the best electrolyte for the electrode material.

6 Concluding Remarks

Commercializing SCs is greatly dependent on their cyclic stability and is one of the basic requirements for industrialization. SCs are now trying to make their place in the electronic industries with key technologies and compete for the future market. There are abundant carbon materials that are commercially available, but by using biomass-derived carbon materials, economic benefits can be gained without sacrificing the cycle life. Taking everything into account, the following points must be kept in mind in order to develop high-performance electrode materials for SCs with high cyclic stability:

(a) The cyclic stability of the SCs device is highly dependent on the electrode materials and their stability. The mechanism of energy storage is dependent on the electrode materials and is a deciding factor for the electrochemical performance.

The cyclic stability dependence on the storage mechanism follows the following order: EDLC > intercalation type SCs > pseudocapacitance.

(b) Optimizing different precursors in order to obtain desired structure, surface properties, and composition by properly assessing the type of electrode material for energy storage, improved cyclic stability can be achieved. For instance, by constructing microstructure morphology and coating or encapsulating ions, nanoparticles, and atoms within the system.

(c) Proper selection of cheap and abundant biomass that possesses a high percentage of carbon, a long shelf life, and is easily scalable

(d) Flexible, microstructured, and wearable SCs have become highly fascinating in recent years. Standard and controlled methods of synthesis are used to produce desired textures and morphologies.

(e) In-depth study of pore size distribution, ion storage and transport, and surface area can guide the preparation of carbonaceous structures with enhanced electrochemical performance.

(f) SCs with high specific capacitance and power density have already been achieved, but enhancing energy density is a matter of research, so using proper electrolytes with wide potential windows must be exploited. Electrolyte philicity is an important matter of study for high cycle life and electrochemical performance. Always, an attempt must be made to maintain equilibrium between the electrode and the electrolyte. If the electrode materials have less electrolyte philicity, the electroactive materials will not get wetted properly, and as a result, adsorption, desorption, or intercalation of the ions during the electrochemical reactions will be hindered. Again, if the electroactive materials are overly wetted by the electrode, structure deformation occurs, impeding electrochemical processes.

(g) Stimulating the natural properties of the biomass, which include self-healability, self-power, environmental stability, and sensitive, sophisticated SCs, can be designed.

(h) Cyclic stability is highly influenced by the test conditions. The scan rate and current density must be almost similar in order to obtain maximum capacitance. The potential must also be consistent with the electrochemical analysis. Therefore, as a whole, the cyclic stability test must be carried out with appropriate parameters.

References

1. Tang X, Wen G, Song Y (2018) Appl Surf Sci 436:398
2. Peurifoy SR, Castro E, Liu F, Zhu XY, Ng F, Jockusch S, Steigerwald ML, Echegoyen L, Nuckolls C, Sisto TJ (2018) J Am Chem Soc 140:9341
3. Wang Y, Wang Z, Chen Y, Zhang H, Yousaf M, Wu H, Zou M, Cao A, Han RP (2018) Adv Mater 30:1802074
4. Sharma K, Arora A, Tripathi SK (2019) J Energy Storage 21:801

5. Eftekhari AJ (2018) Mater Chem A 6:2866
6. Sevilla M, Fuertes AB (2009) Chem Eur J 15:4195
7. Hu B, Wang K, Wu L, Yu SH, Antonietti M, Titirici MM (2010) Adv Mater 22:813
8. Jin H, Li J, Yuan Y, Wang J, Lu J, Wang S (2018) Adv Energy Mater 8:1801007
9. Cui X, Antonietti M, Yu SH (2006) Small 2:756
10. Barroso-Bogeat A, Alexandre-Franco M, Fernández-González C, Macías-García A, Gómez-Serrano V (2014) Phys Chem Chem Phys 16:25161
11. Ren Y, Xu Q, Zhang J, Yang H, Wang B, Yang D, Hu J, Liu Z (2014) ACS Appl Mater Interfaces 6:9689
12. 11. Zhang Q, Gu D, Li H, Xu Z, Sun H, Li J, Wang L, Shen L (2021) Electrochim Acta 367:137455
13. Bi W, Deng S, Tang H, Liu Y, Shen J, Gao G, Wu G, Atif M, AlSalhi M S, Cao G. Sci. China Mater. 8, 2022
14. Liu Y, Jiao Y, Zhang Z, Qu F, Umar A, Wu X (2014) ACS Appl Mater Interfaces 6:2174
15. Samuel E, Joshi B, Kim YI, Aldalbahi A, Rahaman M, Yoon SS (2020) ACS Sustain Chem Eng 8:3697
16. Stott A, Tas MO, Matsubara EY, Masteghin MG, Rosolen JM, Sporea RA, Silva SRP (2020) Energy Environ 3:389
17. Huang Y, Li H, Wang Z, Zhu M, Pei Z, Xue Q, Huang Y, Zhi C (2016) Nano Energy 22:422
18. Marriam I, Wang Y, Tebyetekerwa M (2020) Energy Storage Mater 33:336
19. Yu L, Chen GZ (2016) J Power Sources 326:604
20. Yan S, Abhilash KP, Tang L, Yang M, Ma Y, Xia Q, Guo Q, Xia H (2019) Small 15:1804371
21. Wang M, Xia X, Zhong Y, Wu J, Xu R, Yao Z, Wang D, Tang W, Wang X, Tu J (2019) Chem Eur J 25:3710
22. Yamada H, Nakamura H, Nakahara F, Moriguchi I, Kudo T (2007) J Phys Chem C 111:227
23. Yan J, Wang Q, Wei T, Fan Z (2014) Adv Energy Mater 4:1300816
24. Wang J, Kaskel S (2012) J Mater Chem 22:23710
25. Jin Y, Tian K, Wei L, Zhang X, Guo X (2016) J Mater Chem A 4:15968
26. Chmiola J, Yushin G, Gogotsi Y, Portet C, Simon P, Taberna PL (2006) Science 313:1760
27. Mi J, Wang XR, Fan RJ, Qu WH, Li WC (2012) Energ Fuel 26:5321
28. Ouyang T, Cheng K, Yang F, Zhou L, Zhu K, Ye K, Wang G, Cao D (2017) J Mater Chem A 5:14551
29. Liu S, Xu J, Zhu J, Chang Y, Wang H, Liu Z, Xu Y, Zhang C, Liu T (2017) J Mater Chem A 5:19997
30. Wang C, Wu D, Wang H, Gao Z, Xu F, Jiang K (2017) J Power Sources 363:375
31. Simon P, Gogotsi Y (2013) Capacitive energy storage in nanostructured carbon–electrolyte systems. Acc Chem Res 46(5):1094–1103
32. Chao D, Ouyang B, Liang P, Huong TTT, Jia G, Huang H, Xia X, Rawat RS, Fan H (2018) J Adv Mater 30:1804833
33. Montes-Morán MA, Suárez D, Menéndez JA, Fuente E (2004) Carbon 42:1219
34. Lai F, Miao YE, Zuo L, Lu H, Huang Y, Liu T (2016) Small 12:3235
35. Kale VS, Hwang M, Chang H, Kang J, Chae SI, Jeon Y, Yang J, Kim J, Ko YJ, Piao Y, Hyeon T (2018) Adv Funct Mater 28:1803786
36. Berenguer R, García-Mateos FJ, Ruiz-Rosas R, Cazorla-Amorós D, Morallón E, Rodríguez-Mirasol J, Cordero T (2016) Green Chem 18:1506
37. Shen W, Fan W (2013) J Mater Chem A 1:999
38. Hou J, Cao C, Idrees F, Ma X (2015) ACS Nano 9:2556
39. Niu J, Liu M, Xu F, Zhang Z, Dou M, Wang F (2018) Carbon 140:664
40. Teng Y, Liu E, Ding R, Liu K, Liu R, Wang L, Yang Z, Jiang H (2016) Electrochim Acta 194:394
41. Wei T, Zhang Q, Wei X, Gao Y, Li H (2016) Sci Rep 6:1
42. Qu J, Geng C, Lv S, Shao G, Ma S, Wu M (2015) Electrochim Acta 176:982
43. Chen X, Zhang J, Zhang B, Dong S, Guo X, Mu X, Fei B (2017) Sci Rep 7:1

44. Shi Y, Zhang L, Schon TB, Li H, Fan C, Li X, Wang H, Wu X, Xie H, Sun H, Seferos DS (2017) ACS Appl Mater Interfaces 9:42699
45. Li Z, Xu Z, Wang H, Ding J, Zahiri B, Holt CM, Tan X, Mitlin D (2014) Energy Environ Sci 7:1708
46. Zhang LL, Li HH, Shi YH, Fan CY, Wu XL, Wang HF, Sun HZ, Zhang JP (2016) ACS Appl Mater Interfaces 8:4233
47. Yu X, Wang Y, Li L, Li H, Shang Y (2017) Sci rep 7:1
48. Pang J, Zhang WF, Zhang JL, Zhang HM, Cao GP, Han MF, Yang YS (2018) ChemElectroChem 5:1306
49. Liang J, Jiao Y, Jaroniec M, Qiao SZ (2012) Angew Chem Int Ed 51:11496
50. Zhang X, Yan P, Zhang R, Liu K, Liu Y, Liu T, Wang X (2016) J Mater Chem A 4:19053
51. Seredych M, Idrobo JC, Bandosz TJ (2013) J Mater Chem A 1:7059
52. Park SK, Lee H, Choi MS, Suh DH, Nakhanivej P, Park HS (2018) Energy Storage Mater. 12:331
53. Wahid M, Parte G, Fernandes R, Kothari D, Ogale S (2015) RSC Adv 5:51382
54. Tran HD, Li D, Kaner RB (2009) Adv Mater 21:1487
55. Xue J, Zhao Y, Cheng H, Hu C, Hu Y, Meng Y, Shao H, Zhang Z, Qu L (2013) Phys Chem Chem Phys 15:8042
56. Li Y, Wang G, Wei T, Fan Z, Yan P (2016) Nano Energy 19:165
57. Peng L, Fang Z, Zhu Y, Yan C, Yu G (2018) Adv Energy Mater 8:1702179
58. Lee JH, Park N, Kim BG, Jung DS, Im K, Hur J, Choi JW (2013) ACS Nano 7:9366
59. Bae CJ, Erdonmez CK, Halloran JW, Chiang YM (2013) Adv Mater 25:1254
60. Chen C, Zhang Y, Li Y, Dai J, Song J, Yao Y, Gong Y, Kierzewski I, Xie J, Hu L (2017) Energy Environ Sci 10:538
61. Xiao PW, Meng Q, Zhao L, Li JJ, Wei Z, Han BH (2017) Mater Des 129:164
62. Lyu L, Seong KD, Ko D, Choi J, Lee C, Hwang T, Cho Y, Jin X, Zhang W, Pang H, Piao Y (2019) Mater Chem Front 3:2543
63. Wei Q, Xiong F, Tan S, Huang L, Lan EH, Dunn B, Mai L (2017) Adv Mater 29:1602300
64. Jin Z, Yan X, Yu Y, Zhao G (2014) J Mater Chem A 2:11706
65. Sakurada I, Nukushina Y, Ito T (1962) J Polym Sci 57:651
66. Kang YJ, Chun SJ, Lee SS, Kim BY, Kim JH, Chung H, Lee SY, Kim W (2012) ACS Nano 6:6400
67. Wang Z, Carlsson DO, Tammela P, Hua K, Zhang P, Nyholm L, Strømme M (2015) ACS Nano 9:7563
68. Torvinen K, Lehtimäki S, Keränen JT, Sievänen J, Vartiainen J, Hellén E, Lupo D, Tuukkanen S (2015) Electron Mater Lett 11:1040
69. Li S, Huang D, Yang J, Zhang B, Zhang X, Yang G, Wang M, Shen Y (2014) Nano Energy 9:309
70. Mai L, Tian X, Xu X, Chang L, Xu L (2014) Chem Rev 114:11828
71. Chen W, Yu H, Lee SY, Wei T, Li J, Fan Z (2018) Chem Soc Rev 47:2837
72. 72. Cao Y, Xie L, Sun G, Su F, Kong QQ, Li F, Ma W, Shi J, Jiang D, Lu C, Chen CM (2018) Sustain Energy Fuels 2:455
73. Shi Z, Xing L, Liu Y, Gao Y, Liu J (2018) Carbon 129:819
74. Wang X, Kong D, Zhang Y, Wang B, Li X, Qiu T, Song Q, Ning J, Song Y, Zhi L (2016) Nanoscale 8:9146
75. 75. He S, Chen W (2015) Sustain Energy Fuels 294:150
76. Hina K, Zou H, Qian W, Zuo D, Yi C (2018) Cellulose 25:607
77. Zhang X, Meng X, Gong S, Li P, Jin LE, Cao Q (2016) Mater Lett 179:73
78. Zhang X, Zhang K, Li H, Cao Q, Li P (2017) J Power Sources 344:176
79. Xu W, Mu B, Wang A (2016) Electrochim Acta 194:84
80. Tan C, Cao X, Wu XJ, He Q, Yang J, Zhang X, Chen J, Zhao W, Han S, Nam GH, Sindoro M (2017) Chem Rev 117:6225
81. Liu M, Niu J, Zhang Z, Dou M, Wang F (2018) Nano Energy 51:366
82. Hou Y, Lohe MR, Zhang J, Liu S, Zhuang X, Feng X (2016) Energy Environ Sci 9:478

83. Fan Z, Liu Y, Yan J, Ning G, Wang Q, Wei T, Zhi L (2012) Wei Adv Energy Mater 2:419
84. Mendoza-Sánchez B, Gogotsi Y (2016) Adv Mater 28:6104
85. Yi F, Ren H, Shan J, Sun X, Wei D, Liu Z (2018) Chem Soc Rev 47:3152
86. Liu B, Liu Y, Chen H, Yang M, Li H (2017) J Power Sources 341:309
87. Panmand RP, Patil P, Sethi Y, Kadam SR, Kulkarni MV, Gosavi SW, Munirathnam NR, Kale BB (2018) Nanoscale 10:22065
88. Li Z, Lv W, Zhang C, Li B, Kang F, Yang QH (2015) Carbon 92:11
89. Hou J, Jiang K, Tahir M, Wu X, Idrees F, Shen M, Cao C (2017) J Power Sources 371:148
90. Song S, Ma F, Wu G, Ma D, Geng W, Wan J (2015) J Mater Chem 3:18154
91. Liang Q, Ye L, Huang ZH, Xu Q, Bai Y, Kang F, Yang QH (2014) Nanoscale 6:13831
92. Zhao G, Chen C, Yu D, Sun L, Yang C, Zhang H, Sun Y, Besenbacher F, Yu M (2018) Nano Energy 47:547
93. Li Q, Lu C, Xiao D, Zhang H, Chen C, Xie L, Liu Y, Yuan S, Kong Q, Zheng K, Yin J (2018) ChemElectroChem 5:1279
94. Wang Y, Zhang Y, Pei L, Ying D, Xu X, Zhao L, Jia J, Cao X (2017) Sci Rep 7:41523
95. Zhang ZW, Lu CY, Liu GH, Cao YJ, Wang Z, Yang TT, Kang YH, Wei XY, Bai HC (2022) J Mater Res Technol 19:3034
96. Zhang Y, Yu L, Hu R, Zhang J, Wang Y, Niu R, Qian X, Zhu J (2018) J Mater Chem A 6:17417
97. Fu M, Zhu Z, Zhang Z, Zhuang Q, Chen W, Liu Q (2020) J Alloys Compd 846:156376
98. Cui J, Xi Y, Chen S, Li D, She X, Sun J, Han W, Yang D, Guo S (2016) Adv Funct Mater 26:8487
99. Madhu R, Veeramani V, Chen SM, Manikandan A, Lo AY, Chueh YL (2015) ACS Appl Mater Interfaces 7:15812
100. Ouyang Y, Xing T, Chen Y, Zheng L, Peng J, Wu C, Chang B, Luo Z, Wang X (2020) J Energy Storage 30:101454
101. Wang Y, Liu Y, Chen Z, Zhang M, Liu B, Xu Z, Yan K (2022) GreenChE 3:55
102. Qu K, Chen M, Wang W, Yang S, Jing S, Guo S, Tian J, Qi H, Huang Z (2022) J Colloid Interface Sci 616:584
103. Zhang Y, Wang C, Chen X, Dong X, Meng C, Huang C (2021) ACS Appl Energy Mater 4:9328
104. Zhao X, Zhang L, Murali S, Stoller MD, Zhang Q, Zhu Y, Ruoff RS (2012) ACS Nano 6:5404
105. Li Q, Xu Y, Zheng S, Guo X, Xue H, Pang H (2018) Small 14:1800426
106. Tang Y, Zheng S, Xu Y, Xiao X, Xue H, Pang H (2018) Energy Storage Mater 12:284
107. Wang X, Chen S, Li D, Sun S, Peng Z, Komarneni S, Yang D (2018) ACS Sustain Chem Eng 6:633
108. Yang M, Kim DS, Hong SB, Sim JW, Kim J, Kim SS, Choi BG (2017) Langmuir 33:5140
109. 109. Gogoi D, Karmur RS, Das MR, Ghosh NN (2022) Sustain Energy Fuels 6:3599
110. Wang X, Chu J, Yan H J, Zhang H K (2020) Heliyon 10631
111. Ganesh A, Sivakumar T, Sankar G. (2022) J Mater Sci: Mater Electron 1
112. Teimuri-Mofrad R, Payami E, Piriniya A, Hadi R (2022) Appl Organomet Chem 36:6620
113. Wen T, Wu XL, Zhang S, Wang X, Xu AW (2015) Chem Asian J 10:595
114. Zhang Q, Huang L, Kang S, Yin C, Ma Z, Cui L, Wang Y (2017) RSC Adv 7:43642
115. Wang J, Rao M, Ye C, Qiu Y, Su W, Zheng SR, Fan J, Cai SL, Zhang WG (2020) RSC adv 10:4621
116. Sirisomboonchai S, Kongparakul S, Nueangnoraj K, Zhang H, Wei L, Reubroycharoen P, Guan G, Samart C (2018) Appl Surf Sci 436:639
117. Li ZX, Yang BL, Zou KY, Kong L, Yue ML, Duan HH (2019) Carbon 144:540
118. Hu JR, Zhou JW, Jia YX, Li S (2022) New Carbon Mater 37:412
119. Pandey VK, Verma S, Verma B (2022) Chem Phys Lett 802:139780
120. Sun PP, Li YM, Zhang YH, Shi H, Shi FN (2022) J Alloys Compd 896:163081
121. Nithya VD, Arul NS (2016) J Mater Chem A 4:10767
122. Wu XL, Wen T, Guo HL, Yang S, Wang X, Xu AW (2013) ACS Nano 7:3589
123. Zhang J, Zhao H, Li J, Jin H, Yu X, Lei Y, Wang S (2019) Adv Energy Mater 9:1803221
124. Butnoi P, Pangon A, Berger R, Butt HJ, Intasanta V (2021) J Mater Res Technol 12:2153

125. Venkateswarlu S, Mahajan H, Panda A, Lee J, Govindaraju S, Yun K, Yoon M (2021) Chem Eng J 420:127584
126. Choi W, Choudhary N, Han GH, Park J, Akinwande D, Lee YH (2017) Mater Today Commun 20:116
127. Islam N, Wang S, Warzywoda J, Fan Z (2018) J Power Sources 400:277
128. Guo Y, Zhang Y, Wang Y, Zhang D, Lu Y, Luo R, Wang Y, Liu X, Kim JK, Luo Y (2019) Electrochim Acta 296:989
129. Xiong D, Li X, Bai Z, Lu S (2018) Small 14:1703419
130. Zhang Y, Ruan K, Shi X, Qiu H, Pan Y, Yan Y, Gu J (2021) Carbon 175:271
131. Pu L, Zhang J, Jiresse NKL, Gao Y, Zhou H, Naik N, Gao P, Guo Z (2022) Adv Compos Mater 5:356
132. Sun L, Fu Q, Pan C (2021) J Hazard Mater 410:124565
133. Wei L, Deng W, Li S, Wu Z, Cai J, Luo J (2022) J Bioresour Bioprod 7:63
134. Deng X, Zhao B, Zhu L, Shao Z (2015) Carbon 93:48
135. Ouyang T, Cheng K, Gao Y, Kong S, Ye K, Wang G, Cao D (2016) J Mater Chem A 4:9832
136. Liu X, Antonietti M (2014) Carbon 69:460
137. Kamali AR, Fray D (2015) J Chem Commun 51:5594
138. Liu X, Giordano C, Antonietti M (2014) Small 10:193
139. Wang J, Nie P, Ding B, Dong S, Hao X, Dou H, Zhang X (2017) J Mater Chem A 5:2411
140. Ouyang T, Cheng K, Yang F, Zhou L, Zhu K, Ye K, Wang G, Cao DJ (2017) Mater Chem A 5:14551